



Changes in HIRS Detection of Cloud over Australia from 1985 to 2001

Helen Chedzey ^{1,*}, W. Paul Menzel ² and Mervyn Lynch ¹

¹ Remote Sensing and Satellite Research Group, Curtin University, Perth 6102, Australia; m.lynch@curtin.edu.au

² Cooperative Institute for Meteorological Satellite Studies, University of Wisconsin-Madison, Madison, WI 53706, USA; paulm@ssec.wisc.edu

* Correspondence: helen.chedzey@curtin.edu.au

Abstract: A long-term archive of cloud properties (cloud top pressure, CTP; and cloud effective emissivity, ϵ) determined from High-resolution Infrared Radiation Sounder (HIRS) data is investigated for evidence of regional cloud cover change. In the 17 years between 1985 and 2001, different cloud types are analysed over the Australian region (10° S–45° S, 105° E–160° E) and areas of change in total cloud frequency examined. Total cloud frequency change over the Australian region between two adjacent eight-year time periods (1994 to 2001 minus 1985 to 1992) shows the largest increases (ranges between 6% and 12%) of average HIRS total cloud cover occurring over the offshore regions to the northwest and northeast of the continent. Over land, the largest reduction of average HIRS total cloud frequency is in the southwestern region of Australia (between 2% and 8%). Through central Australia, there is a 2% to 7% increase in average HIRS total cloud frequency when comparing these eight-year periods. This paper examines the regional cloud changes in 17 years over Australia that are embedded in global cloud statistics. Examining total HIRS cloud cover frequency over Australia and comparing two different eight-year time periods, has highlighted notable areas of average change. Preliminary reporting of satellite-derived HIRS cloud products and Global Precipitation Climatology Project (GPCP) rainfall products during La Niña seasons between 1985 and 2001 has also been undertaken.

Keywords: HIRS; cloud; cloud properties; GPCP; Australia; regional; remote sensing



Citation: Chedzey, H.; Menzel, W.P.; Lynch, M. Changes in HIRS Detection of Cloud over Australia from 1985 to 2001. *Remote Sens.* **2021**, *13*, 917. <https://doi.org/10.3390/rs13050917>

Academic Editor: Filomena Romano

Received: 29 December 2020

Accepted: 23 February 2021

Published: 1 March 2021

Publisher's Note: MDPI stays neutral with regard to jurisdictional claims in published maps and institutional affiliations.



Copyright: © 2021 by the authors. Licensee MDPI, Basel, Switzerland. This article is an open access article distributed under the terms and conditions of the Creative Commons Attribution (CC BY) license (<https://creativecommons.org/licenses/by/4.0/>).

1. Introduction

Since the first cloud-observing satellite was launched in 1959, numerous generations of satellites and instruments have contributed to the creation of large archives of physical and microphysical cloud data. As satellites have performed beyond lifespan specifications and the continuity of subsequently launched platforms, research into clouds and weather systems has expanded from comprehensive short-term analysis to include long-term climate trends.

A number of long-term cloud data archives exist within the Advanced Very High-Resolution Radiometer (AVHRR) Pathfinder Atmospheres–Extended (PATMOS-x) program [1], the International Satellite Cloud Climatology Project (ISCCP) [2], and the University of Wisconsin/National Oceanic and Atmospheric Administration (UW/NOAA) Pathfinder High-resolution Infrared Radiation Sounder (HIRS) data archive [3].

As the spectral range of the respective instruments and the methodologies used to interpret the sensor information can be different, a thorough comparison among different climatologies was reported by the Global Energy and Water Cycle Experiment (GEWEX) Cloud Assessment Project [4]. Along with AVHRR, ISCCP, and HIRS data, results from numerous other data sets such as MODIS (Moderate-resolution Imaging Spectroradiometer), AIRS (Atmospheric Infrared Sounder), CALIPSO (Cloud-Aerosol Lidar and Infrared Pathfinder Satellite Observations), and CloudSat were reported.

While the HIRS data was reported to show low sensitivity in detecting low-level land-based clouds [4], it performed strongly in detecting high, thin clouds. This is a feature of the CO₂ slicing method; a technique that takes advantage of the placement of the HIRS infrared bands around the 15 µm CO₂ absorption band and uses the raw data to algorithmically determine a number of defining cloud parameters [5].

The general summary of global cloud cover from the different data sets assessed in the GEWEX paper [4] indicate a global cloud coverage of 68% (±3%) for clouds with an optical depth greater than 0.1. Of the total amount of clouds detected, 45% (±5%) of these are high-level clouds, 15% (±5%) of the total are mid-level clouds and 40% (±3%) of the total number of clouds are low-level clouds.

The HIRS data analysed by Wylie et al. [6] report a slightly higher global cloud coverage of 75%, comprising 33% high-level clouds (44% of the total), 18% mid-level clouds (24% of the total), and 24% low-level clouds (32% of the total). The difference from the general GEWEX summary shows that using the HIRS CO₂ slicing method, fewer clouds are observed at a low-level (percentage of total) and a higher number of clouds (percentage of total) are classified as mid-level.

An ISCCP (International Satellite Cloud Climatology Project) study by Rossow et al. [7] reported on global cloud summaries and the differing regional results highlighted by the geographical distribution of clouds across the globe. Using the HIRS data set, the differences between the cloud cover observed over Australia and the global HIRS product by Wylie are analysed. Regional changes in cloud cover over time in Australia are then investigated and compared to GPCP (Global Precipitation Climatology Project) data.

The motivation for this study is to further research reports of long-term reduced cloud and rainfall, particularly in the southwest of Western Australia [8]. This paper investigates what variability of HIRS cloud cover occurs across regions of Australia and whether there are discernible trends in those regions that can be associated with rainfall change.

2. Materials and Methods

The HIRS data archive consists of radiometric measurements recorded from four different generations of the HIRS instrument [9] beginning in the late 1970s through to present day. The following cloud analysis focusses on data retrieved from the HIRS/2 instrument that was aboard satellites NOAA-5 through to NOAA-14 (operational during the period 1979 to 2001).

The measurements recorded by the HIRS/2 instrument exist for 20 different spectral bands, 19 within the infrared spectral region (ranging between 3.7 µm and 15 µm) and one in the visible spectrum (at 700 nm) [10].

Five of the narrow sensor spectral bands selected along the transmission/absorption boundary of the 15 µm CO₂ absorption band are able to detect different depths of the atmosphere. The data collected from these infrared bands are then applied through the CO₂ slicing method to derive cloud parameters.

The CO₂ slicing algorithm was theorised by Chahine [11] and Smith et al. [12] with some initial successful validation results of cloud height derived using this method reported by Smith and Platt [13]. Further validation was conducted by Menzel et al. [14] and Frey et al. [15]. The technique has been outlined in detail in Wylie et al. [5] and can be briefly summarised as being based on the radiative transfer equation for a single cloud layer in the atmosphere that aims to obtain measurements of cloud top pressure (CTP) and effective emissivity (ϵ). When considering observed radiance incident on a satellite sensor, the contributions from a clear field-of-view (FOV) would be divided between radiance from the Earth's surface and radiance from the atmosphere. If a cloud is present, the radiation would come from the Earth's surface, from the atmosphere below the cloud and above the cloud, and also from the cloud itself. By finding the difference between the clear FOV radiance and the cloud observed radiance, the cloud contribution can be determined. In order to reveal clouds at different atmospheric levels, specific combinations of spectrally close bands (between 13 µm and 15 µm and adjacent to the CO₂ absorption band) are used.

The HIRS/2 data provided by Wylie [16], generated by the CO₂ slicing algorithm, were the uncorrected average counts of monthly cloud observations for each satellite with a 1° latitude/longitude resolution. Apart from the total number of cloud observations and the total number of clear sky observations observed during each month, cloud observations were also arranged into combinations of nine different divisions of cloud height and six different divisions of cloud emissivity. Data were initially examined from the ascending orbit satellites (NOAA-5, NOAA-7, NOAA-9, NOAA-11, and NOAA-14) with a local equator crossing time in the early afternoon that offered a continuous data record.

Unexplained performance issues with NOAA-7 during the early 1980s were noted in Wylie et al. [6] and this has led to the HIRS analysis conducted here to focus only on the consecutive data collected between 1985 and 2001 from three satellites, NOAA-9, NOAA-11, and NOAA-14.

When assessing changes in cloud frequency observations and changes in rainfall, the Global Precipitation Climatology Project (GPCP) data set was selected as a precipitation data source with similar spatial and temporal attributes to the available HIRS cloud products. GPCP development is described in Adler et al. [17], Huffman et al. [18], Huffman and Bolvin [19], and Adler et al. [20]. The Version 2.3 monthly precipitation product merges rain-gauge data with satellite-derived rainfall estimated from several different microwave and infrared sensor observations and was sourced online from the NOAA Earth System Research Laboratory [21].

When assessing seasons with above- and below-average rainfall, different cloud types and classifications from El Niño and La Niña seasonal months are investigated to provide a clearer understanding of the type of clouds associated with rainfall.

The El Niño Southern Oscillation (ENSO) is described as a coupled ocean-atmosphere system with two distinct phases that can affect weather patterns in tropical and subtropical climates, the warm phase called El Niño and the cold phase, La Niña [22].

The oceanic aspect of the ENSO system involves sea surface temperature (SST) anomalies. The Oceanic Niño Index (ONI) calculates three-month running means of sea surface temperature (SST) anomalies determined for a particular oceanic region; the Niño 3.4 region (5° N–5° S, 120° W–170° W) [23]. If the mean anomaly exceeds 0.5° C for more than five consecutive index values, the contributing months are deemed a warm episode. A cold episode is determined by five continuous index values registering less than −0.5° C.

The atmospheric part of the ENSO system involves mean sea level pressure (MSLP) differences. The Southern Oscillation Index (SOI) is determined from the mean sea level pressure (MSLP) difference between Tahiti in the central Pacific Ocean and Darwin, Australia (MSLP difference = Tahiti – Darwin) [24]. During an El Niño event, the SOI experiences negative values (higher surface pressure over Darwin) and higher than normal ocean temperatures in the eastern Pacific Ocean. La Niña events have positive values of the SOI (high surface pressure over Tahiti) combined with cooler eastern Pacific Ocean temperatures.

An El Niño event within Australia often means lower than average levels of rainfall while a La Niña event would usually be associated with higher-than-average levels of rainfall. In order to determine the El Niño and La Niña events that occurred between 1985 and 2001, a combination of SOI values and variations in the NCEP/NOAA Oceanic Niño Index (ONI) were assessed. The defined events used in this study are outlined in Table 1.

Table 1. El Niño and La Niña events between 1985 and 2001 determined by assessing Oceanic Niño Index and Southern Oscillation Index historical values.

EL NIÑO	LA NIÑA
August 1986–February 1988	May 1988–June 1989
April 1991–July 1992	June 1998–April 2001
August 1994–April 1995	
April 1997–April 1998	

While low Earth orbit platforms target a specific local overpass time upon launch, after many years of operation, the equator crossing times (EXT) of satellites can change. After launch, the early NOAA satellites EXT shifted from their original orbits. Adjusting the satellite radiometric data for orbit drift ensures cloud frequency observations can be compared at the same time of day over extended periods. The HIRS data in this analysis were collected between 1985 and 2001 aboard three afternoon satellites, NOAA-9, NOAA-11, and NOAA-14. Using the platform parameters tabled in Ignatov et al. [25], the drift of each of these satellites was calculated and is shown in Figure 1.

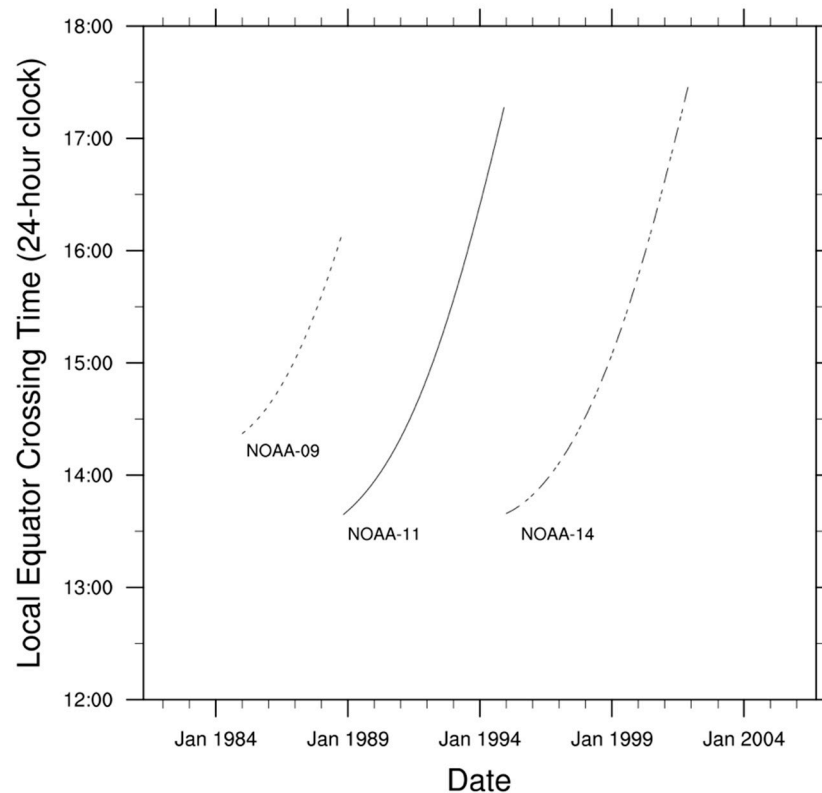


Figure 1. Evolution of orbit drift in the local equator crossing time of NOAA-09, -11, and -14 afternoon satellites between 1985 and 2001.

Similar to the procedure in Wylie et al. [6], scatter plots of cloud frequency and EXT were generated for all combinations of the HIRS cloud categories (high, mid and low; thin, thick and opaque) over the Australian region (10° S– 45° S, 105° E– 160° E) for the lifetime of each platform.

The linear cloud frequency changes per hour of satellite orbit drift were determined from each plot then used to linearly-correct the cloud frequency data from each platform to a 2 pm EXT. The orbit drift adjustment was applied to the HIRS cloud data prior to any analysis being conducted.

Overall, the orbit drift corrections had little influence on the summarised Australian cloud frequencies. High cloud frequency observations remained unaltered while there were minor increases calculated in mid- and low-level cloud observations. The main effects of the orbit drift corrections were seen in the low opaque cloud observation category where an overall increase of 1% resulted from the orbit drift corrections. A slight increase was calculated for mid-level cloud leading to a 1% increase due to rounding. This has led to the total cloud frequency observations over Australia increasing by 2% (by rounding) from 56% to 58% after the data was corrected for orbit drift (see Table 2).

Table 2. Australian region (10° S–45° S, 105° E–160° E) region cloud frequency summary for the HIRS/2 sensor series showing uncorrected results and those corrected for orbit drift. The statistics categorise differing cloud height observations over land.

Australia:	ALL CLOUD	HIGH CLOUD <440 hPa	MID CLOUD >440 hPa, <700 hPa	LOW CLOUD >700 hPa
UNCORRECTED	56%	25%	9%	22%
CORRECTED	58%	25%	10%	23%

The HIRS cloud parameters are calculated (via the CO₂ slicing algorithm) using a static CO₂ value of 380 ppm. In reality, CO₂ levels within the atmosphere have changed over time. At the beginning of the HIRS/2 data archive in 1979 the CO₂ value was 335 ppm and by the end of 2001, the CO₂ value had increased to 375 ppm. While the CO₂ difference wasn't corrected for in this study, Wylie et al. [6] discuss the effect that the difference in CO₂ has on the algorithm performance. Wylie suggests that the clouds detected in earlier years are slightly too high (by 13 hPa–50 hPa). Accordingly, any high cloud frequency differences calculated using this data, between two adjacent eight-year periods will therefore be slightly underestimated.

3. Results

The Wylie data [16] reported 75% cloud coverage globally [6]. When reprocessed for the Southern region of the globe (20° S–60° S) and separated into land and ocean statistics, all cloud over land was observed 64% of the time and over ocean, 80% of the time.

Over the Australian region (10° S–45° S, 105° E–160° E), all cloud was observed over land 58% of the time (see Table 2). This is a reduction of 17% from the global cloud coverage observed over land and ocean, and a reduction of 6% from the Southern region cloud coverage observed over land.

High-level cloud was observed at 25% (43% of the total) over Australia with mid-level cloud being observed 10% of the time (17% of the total) and low-level cloud observed 23% of the time (40% of the total). The high-, mid-, and low-level percentage ratios of total cloud observed over Australia are shown to align more with the GEWEX results (45-15-40) than the elevated mid-level and reduced low-level ratios seen in the HIRS global results (44-24-32).

Images created using the 17-year archive (1985–2001) of HIRS data provide an opportunity to examine the geographical distribution of cloud observations over Australia and how they vary among the seasons. Figure 2 illustrates the average seasonal results of total cloud frequency over the Australian region.

During the summer months (December, January, and February) there exists an onset and retreat of monsoonal cloud cover over northern Australia. A region of diminished continental cloud cover occurs during the winter months (June, July, and August) over the northern half of the continent and over the north-west ocean region. The area affected contracts during the spring months (September, October, and November) to the north-west coast of Western Australia.

This latter extended period of infrequent cloud cover is consistent with the Gascoyne region of Western Australia being the most cloud-free region in Australia. Research conducted by Udelhofen et al. [26] reported the mid-west region of Western Australia (bounded by the latitudes of 20° S and 30° S which incorporates the Gascoyne and Pilbara regions) to have the lowest annual average percentage of cloud cover (33.7% ± 3.7%) when compared to 13 other Australian regions. These results were calculated from 14 years of TOMS (NASA Total Ozone Mapping Spectrometer) data between 1979 and 1992.

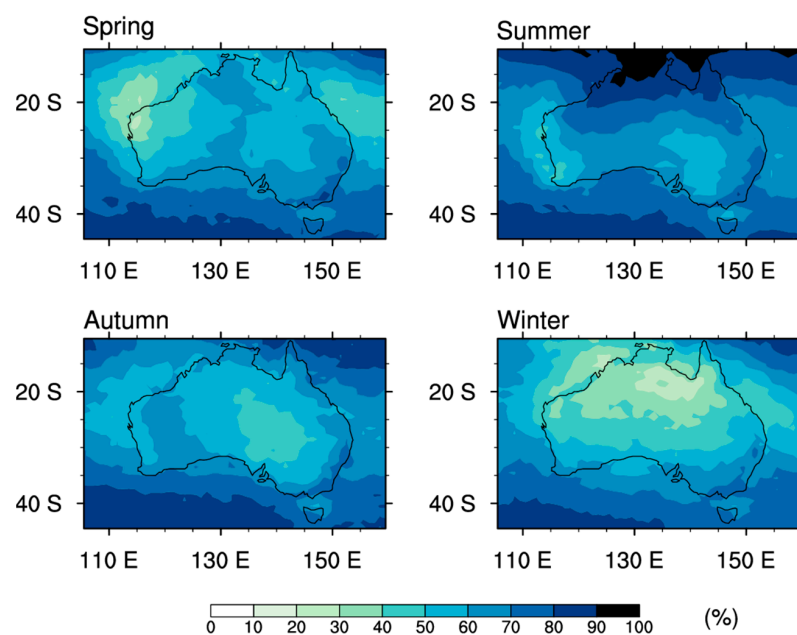


Figure 2. Total cloud observation percentage images, seasonally averaged over 17 years of HIRS data (1985–2001) for the Australian region (10° S– 45° S, 105° E– 160° E). Images separated into Southern Hemisphere spring months (**top left**), summer months (**top right**), autumn months (**bottom left**) and winter months (**bottom right**).

Analysing an extended period of HIRS data allows for a comparison between two separate time periods where any systematic trends in cloud frequency might be highlighted. For the 17 years between 1985 and 2001, an initial eight-year period consists of averaged HIRS cloud frequency data between the years of 1985 and 1992. A second eight-year period averages HIRS cloud frequency data between 1994 and 2001. Figure 3 illustrates the differences in HIRS total cloud frequency between these two periods by subtracting the averaged data for 1985 to 1992 from the more recently averaged data for the period 1994 to 2001. An overlaid reference of state boundaries and regional locations across Australia are also included in Figure 3.

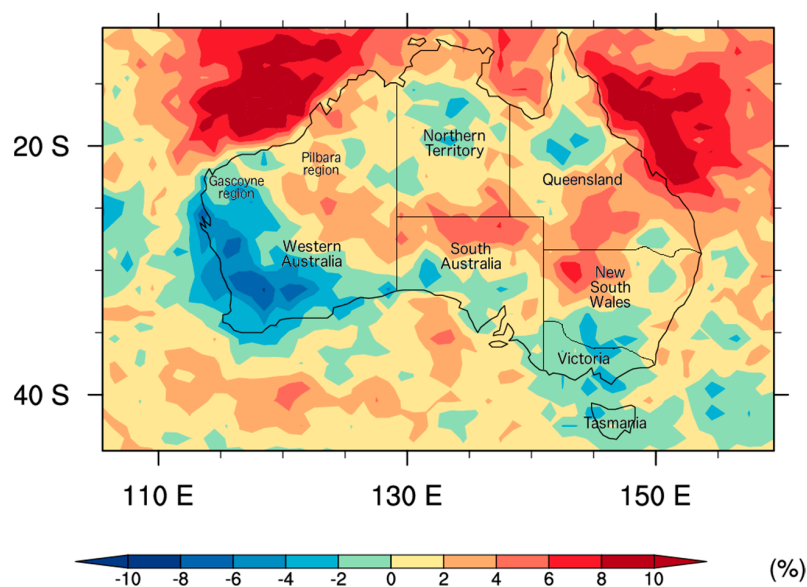


Figure 3. Change in average HIRS total cloud frequency % between two different eight-year periods for the Australian (10° S– 45° S, 105° E– 160° E) region. Difference = (1994–2001) minus (1985–1992).

Figure 3 shows the largest increases in average total cloud cover, from the earlier eight-year period to the more recent eight-year period, occurring over the waters to the northwest and northeast of the Australian continent (between 6% and 12%). Smaller increases (between 2% and 7%) in average total cloud frequency occur over the central region of Australia.

Small reductions of average total cloud frequency over time, up to 2% and 3%, are observed over southern South Australia, Tasmania, the southeast corner of Australia and smaller zones within the Northern Territory and Northern Queensland.

In Western Australia, there are two distinct areas of total cloud cover change. The largest reduction of average total cloud frequency between the two temporal periods in Figure 3 (shown in blue) is seen to cover a substantial area of southwestern and mid-western Australia. The average cloud frequency of total cloud during the latter part of the 1990s (between 1994 and 2001) was between 2% and 8% less than the average cloud frequency observed in the late 1980s (1985 to 1992). The two primarily offshore regions (centred on 17° S, 118° E) off the NW coast and off the NE coast (centred on 20° S, 150° E) show an increase in cloud cover frequency of up to 12%.

Changes in rainfall across Australia can also be depicted by differences between the same two adjacent eight-year time periods. An attempt was made to determine the types of clouds best associated with geographic differences in rainfall during El Niño and La Niña seasons.

Table 3 examines the observational frequencies of total cloud as well as the frequency of high clouds for the Australian region. Summaries are detailed for three different subsets of data; the entire 17-year archive, El Niño years and La Niña years. Over the entire 17-year archive, cloud of any type is observed 58% of the time over the Australian continent. During El Niño seasons the cloud observation percentage remains the same as the archival value, 58%, while the La Niña season frequency increases to 60%.

Table 3. The Australian region (10° S–45° S, 105° E–160° E) cloud frequency observations of total cloud and high cloud (CTP < 440 hPa) over land. Observations from La Niña and El Niño years are summarised and compared with the cloud frequency percentages taken from the full HIRS data set (1985 through to 2001).

Australia:	ALL DATA (1985–2001)	EL NIÑO (8/1986–2/1988, 4/1991–7/1992, 8/1994–4/1995, 4/1997–4/1998)	LA NIÑA (5/1988–6/1989, 6/1998–4/2001)
TOTAL CLOUD	58%	58%	60%
HIGH CLOUD	25%	25%	27%

After expanding the total cloud frequencies into different height classifications, the leading influence behind the increased La Niña total cloud frequency values is seen in the high cloud (CTP < 440 hPa) frequency summaries. Listed in Table 3, the archive high cloud observation percentage is 25%. The La Niña high cloud observation percentage is 27%; 2% higher than the archival and the El Niño high cloud observation percentages.

High clouds are then categorised as thin, thick, or opaque and the calculated frequencies from the HIRS data for El Niño and La Niña seasons are summarised in Table 4. La Niña season high thick clouds are observed 15% of the time, a frequency 3% higher than in the El Niño seasons and 2% higher than the 17-year archive.

Table 4. The Australian region (10° S– 45° S, 105° E– 160° E) cloud frequency observations of high thin (CTP < 440 hPa; $\epsilon < 0.5$), high thick (CTP < 440 hPa; $0.5 < \epsilon < 0.95$) and high opaque (CTP < 440 hPa; $\epsilon > 0.95$) clouds over land. Observations from La Niña and El Niño years are summarised and compared with the cloud frequency percentages taken from the full HIRS data set (1985 through to 2001).

Australia:	ALL DATA (1985–2001)	EL NIÑO (8/1986–2/1988, 4/1991–7/1992, 8/1994–4/1995, 4/1997–4/1998)	LA NIÑA (5/1988–6/1989, 6/1998–4/2001)
HIGH THIN	11%	11%	11%
HIGH THICK	13%	12%	15%
HIGH OPAQUE	1%	1%	1%

The differences in high thick clouds between common months within the La Niña and El Niño seasons are illustrated in Figure 4. While El Niño events are associated with lower–than–average rainfall and La Niña events are associated with higher–than–average rainfall, the influence of these ENSO phases, within Australia, centre around the eastern and northern regions of the continent. Higher than average levels of rainfall would be expected in these areas of the country during La Niña events and lower than average rainfall expected during El Niño events. If increasing levels of high thick clouds are associated with La Niña rainfall then a response from the La Niña/El Niño difference on the East coast of Australia should be seen.

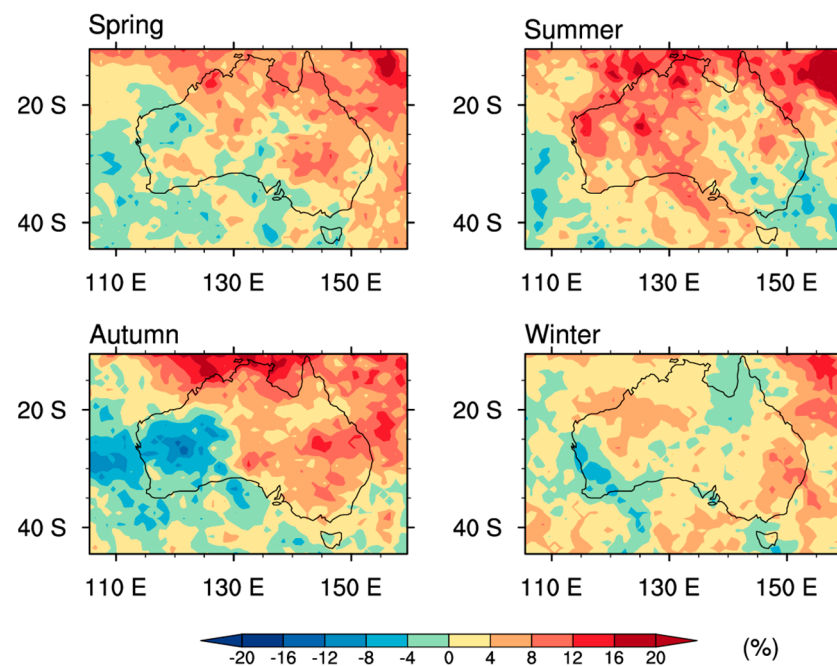


Figure 4. The difference in HIRS high thick (CTP < 440 hPa; $0.5 < \epsilon < 0.95$) cloud observation percentages between La Niña seasons and El Niño seasons selected during the period 1985 to 2001 for the Australian region (10° S– 45° S, 105° E– 160° E). Data summarised from four El Niño seasons (August 1986–February 1988, April 1991–July 1992, August 1994–April 1995 and April 1997–April 1998). Data summarised from two La Niña seasons (May 1988–June 1989 and June 1998–April 2001). Difference = La Niña–El Niño. Images separated into Southern Hemisphere spring months (**top left**), summer months (**top right**), autumn months (**bottom left**) and winter months (**bottom right**) from El Niño and La Niña seasons.

While there is no consistent, all–season, positive difference indicating higher levels of high thick clouds present in La Niña–classified months than El Niño–classified months

on the east coast of Australia in Figure 4, Spring and Autumn show the largest spatial areas where this is the case. The western half of Australia also shows positive high thick cloud/La Niña differences during Summer.

One notable negative cloud frequency difference in the seasonal images of Figure 4 is in Autumn (March, April, and May), in the southern half of Western Australia. The ENSO season classification highlighted negative cloud frequency differences in this area (indicating El Niño classified months reported a higher presence of high thick clouds than La Niña classified months). Rainfall in this area is not greatly affected by the ENSO processes [27].

Figures 5 and 6 show the investigation into the changes in average high thick cloud between two selected eight-year periods (average between 1994 and 2001 minus the average between 1985 and 1992) and the differences in average rainfall for the same periods. The rainfall data were sourced from the Global Precipitation Climatology Project (GPCP) Version 2.3 data set.

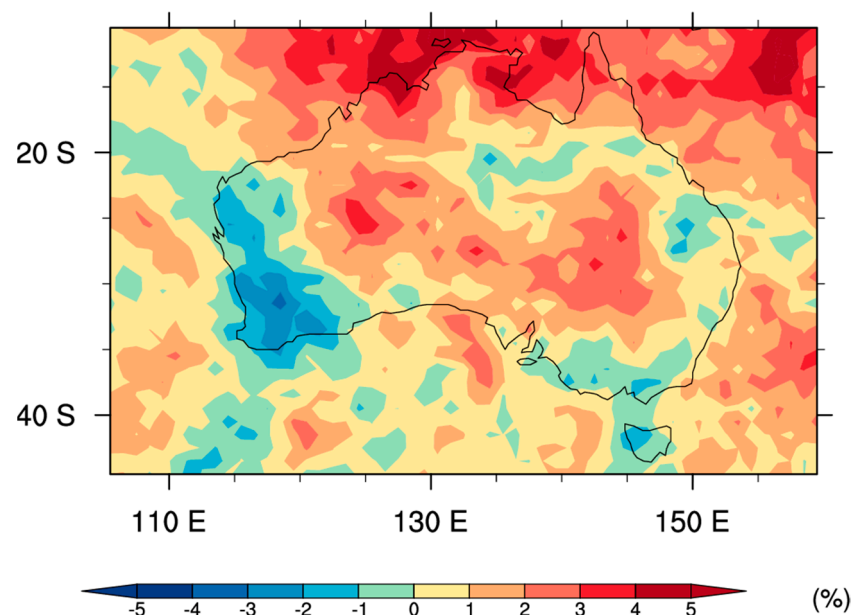


Figure 5. Change in the average cloud frequency of HIRS high thick (CTP < 440 hPa; $0.5 < \varepsilon < 0.95$) between two different eight-year periods for the Australian region (10° S– 45° S, 105° E– 160° E). Difference = (1994–2001) minus (1985–1992).

Average frequency of high thick cloud cover over the northern parts of the Northern Territory and Queensland and over the northern waters of Australia are 2% to 5% higher in the second temporal period (1994–2001) when compared to the first temporal period (1985–1992) (Figure 5). There is also an increase in rainfall in these areas of between 18 mm and 30–35 mm (Figure 6). Across the centre of Australia, there is again the E–W band that experiences a 2% to 3% increase in high thick clouds along with between 4 mm and 20 mm increase in rainfall.

Decreases in the average frequency of high thick clouds (shown in blue in Figure 5, where there are more clouds present between 1985 and 1992 than between 1994 and 2001) are found in two main zones in Figure 5. The main zone is on the west coast of the country while lesser decreases are distributed along the full extent of the east coast.

The area spanning between the Gascoyne region and the southern coastline of Western Australia (20° S to 35° S) experiences up to a 3% reduction in high thick cloud.

Looking at the same zone in Figure 6, the GPCP rainfall shows a small decrease (approximately 3 mm–4 mm) in rainfall for the southwest corner but a slight increase (approximately 6 mm) for the remaining part of the reduced high thick cloud zone.

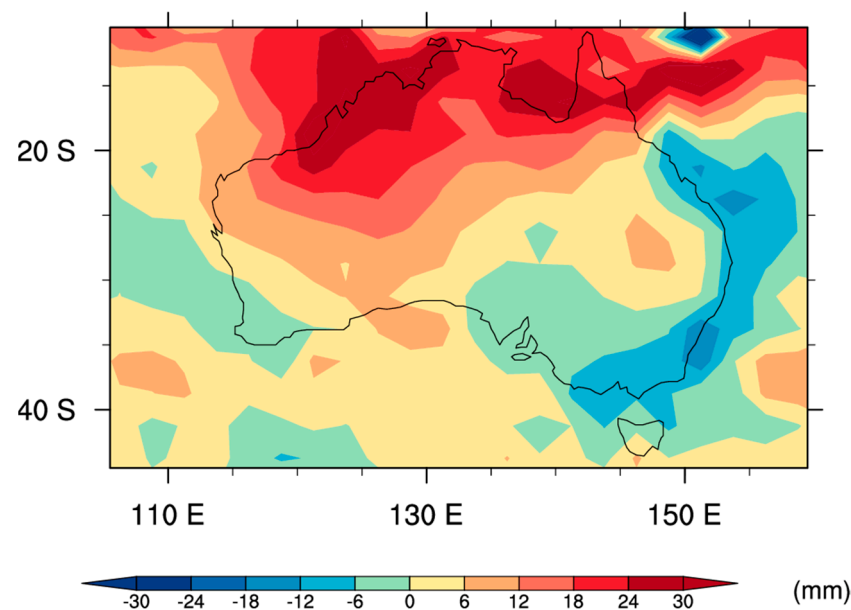


Figure 6. Change in GPCP rainfall between two different eight-year periods for the Australian region (10° S– 45° S, 105° E– 160° E). Difference = (1994–2001) minus (1985–1992).

In Figure 5, the eastern side of Australia contains areas (Tasmania, Victoria, and the southeast corner of Queensland) that show up to a 2% decrease in high thick clouds. Figure 6 shows decreases of GPCP rainfall all along the eastern coastline, in some areas up to 18 mm.

A question remains—how significant are the cloud changes that are reported here? Frey and Menzel [28] reported the mean absolute monthly changes of HIRS-derived, high cloud frequency are “ -0.2% (with scatter about those means from 15.5% to 18.4%) . . . Clearly there is considerable variability in the monthly means from year to year”. This implies that when you average over eight years the scatter gets reduced by an order of magnitude, so changes greater than 2% can be considered significant and less than 2% near random.

4. Discussion and Conclusions

The initial motivation for this research was to undertake a study of regional changes in cloud climatology across Australia.

Figure 3 in this work reveals that the regional scale processes that we have observed suggest there are significant processes at work that are seriously impacting the regional cloud climatology of Australia and that the direction of trends being observed are sustained over significant timescales. The magnitudes of these changes, as shown in Figure 3, are up to 12%; surprisingly large over this relatively short period of observation. The increasing cloud cover is shown to occur predominantly over oceanic regions in latitudes from $\sim 10^{\circ}$ S to $\sim 22^{\circ}$ S with the trends for the NW and NE regions well correlated.

We find that the cloud cover over the bulk of continental Australia shows (in Figure 3) large regions of cloud cover reduction over the 17-year observing period. These areas primarily correspond to Australia’s agriculturally productive regions which is a very significant concern if these trends continue. It is, in a sense, anomalous that the only regions of increased continental cloud cover occur over the extensive desert and low productivity Australian rangelands. The extensive SW region of the Australian continent (from 22° S to 35° S by 112° E to 125° E), of area $\sim 1.5 \times 10^6$ km², shows the largest reduction in cloud cover in the order of $\sim 2\%$ to 8%. The GPCP precipitation data (Figure 6) shows a small average decrease (~ 3 mm– 4 mm) in rainfall for the southwest corner of this region but a slight increase (~ 6 mm) for the remaining area of the SW zone. Again, this is a concerning

trend since this southwest corner is a major agricultural area typically producing 30% to 40% of the national cereal crop.

The preliminary examination of HIRS high thick cloud cover frequency (Figure 5) and the GPCP precipitation pattern (Figure 6) shows that a spatial relationship is evident. There are some regions where the links between the selected cloud parameters and rainfall are not clear, and it would suggest that further investigation into other cloud parameters is necessary. The addition of agricultural productivity data would also provide useful information.

In conclusion, we find that cloud cover changes over these 17 years are regionally defined and argue that continuing regional investigations such as that reported here are important given the timescale of change, the magnitudes of change, and the spatial scales of impacted areas.

5. Future Outlook

There is the prospect of improved cloud diagnostic tools from future on-orbit instruments that should aid an improved understanding of cloud microphysics and associated precipitation. The modelling of clouds and their role in climate change into the future remain a challenging and productive area for research that may identify the sources of the observed changes in cloud cover and give guidance as to what we should expect in the future.

Author Contributions: Conceptualization and methodology, H.C., W.P.M. and M.L.; software and data curation, H.C.; formal analysis and investigation, H.C., W.P.M. and M.L.; writing—original draft preparation, H.C.; writing—review and editing, H.C., W.P.M. and M.L. All authors have read and agreed to the published version of the manuscript.

Funding: This research was partially funded by NOAA, grant number NA06GP0307.

Institutional Review Board Statement: Not applicable.

Informed Consent Statement: Not applicable.

Data Availability Statement: The HIRS data are available from the corresponding author upon request. The GPCP precipitation data are available from the NOAA/OAR/ESRL PSL, Boulder, Colorado, U.S.A. from their website at <http://www.psl.noaa.gov/data/gridded/data.gpcp.html>.

Acknowledgments: Our thanks to Don Wylie for his advice and assistance in providing the HIRS monthly cloud retrievals.

Conflicts of Interest: The authors declare no conflict of interest.

References

1. Heidinger, A.K.; Foster, M.J.; Walther, A.; Zhao, X. The Pathfinder Atmospheres–Extended AVHRR climate dataset. *Bull. Am. Meteor. Soc.* **2014**, *95*, 909–922. [[CrossRef](#)]
2. Rossow, W.B.; Schiffer, R.A. ISCCP cloud data products. *Bull. Am. Meteor. Soc.* **1991**, *72*, 2–20. [[CrossRef](#)]
3. Menzel, W.P.; Frey, R.A.; Borbas, E.E.; Baum, B.A.; Cureton, G.; Bearson, N. Reprocessing of HIRS satellite measurements from 1980 to 2015: Development toward a consistent decadal cloud record. *J. Appl. Meteor. Climatol.* **2016**, *55*, 2397–2410. [[CrossRef](#)]
4. Stubenrauch, C.J.; Rossow, W.B.; Kinne, S.; Ackerman, S.; Cesana, G.; Chepfer, H.; Girolamo, L.D.; Getzewich, B.; Guignard, A.; Heidinger, A.; et al. Assessment of global cloud datasets from satellites: Project and database initiated by the GEWEX radiation panel. *Bull. Am. Meteor. Soc.* **2013**, *94*, 1031–1049. [[CrossRef](#)]
5. Wylie, D.P.; Menzel, W.P.; Woolf, H.M.; Strabala, K.I. Four years of global cirrus cloud statistics using HIRS. *J. Clim.* **1994**, *7*, 1972–1986. [[CrossRef](#)]
6. Wylie, D.; Jackson, D.L.; Menzel, W.P.; Bates, J.J. Trends in global cloud cover in two decades of HIRS observations. *J. Clim.* **2005**, *18*, 3021–3031. [[CrossRef](#)]
7. Rossow, W.B.; Walker, A.W.; Garder, L.C. Comparison of ISCCP and other cloud amounts. *J. Clim.* **1993**, *6*, 2394–2418. [[CrossRef](#)]
8. Pitman, A.J.; Narisma, G.T.; Pielke, R.A.; Holbrook, N.J. Impact of landcover change on the climate of southwest Western Australia. *J. Geophys. Res. Atmos.* **2004**, *109*, 1–12. [[CrossRef](#)]
9. OSCAR: Observing Systems Capability Analysis and Review Tool, World Meteorological Organization. Available online: <https://www.wmo-sat.info/oscar/instruments> (accessed on 10 March 2020).

10. High-Resolution Infrared Radiation Sounder, NASA Space Science Data Coordinated Archive. Available online: <https://nssdc.gsfc.nasa.gov/nmc/experimentDisplay.do?id=1975-052A-02> (accessed on 17 January 2017).
11. Chahine, M.T. Remote sounding of cloudy atmospheres. I. The single cloud layer. *J. Atmos. Sci.* **1974**, *13*, 233–243. [[CrossRef](#)]
12. Smith, W.L.; Woolf, H.M.; Abel, P.G.; Hayden, C.M.; Chalfant, M.; Grody, N. *Nimbus 5 Sounder Data Processing System. I. Measurement Characteristics and Data Reduction Procedures*; NOAA Technical Memorandum, NESS 57; National Oceanic and Atmospheric Administration: Washington, DC, USA, 1974; p. 99.
13. Smith, W.L.; Platt, C.M.R. Comparison of satellite-deduced cloud heights with indications from radiosonde and ground-based laser measurements. *J. Appl. Meteor.* **1978**, *17*, 1796–1802. [[CrossRef](#)]
14. Menzel, W.P.; Smith, W.L.; Stewart, T.R. Improved cloud motion wind vector and altitude assignment using VAS. *J. Appl. Meteor.* **1983**, *22*, 377–384. [[CrossRef](#)]
15. Frey, R.A.; Baum, B.A.; Menzel, W.P.; Ackerman, S.A.; Moeller, C.C.; Spinhirne, J.D. A comparison of cloud top heights computed from airborne lidar and MAS radiance data using CO₂ slicing. *J. Geophys. Res.* **1999**, *104*, 24547–24555. [[CrossRef](#)]
16. Wylie, D.; (University of Wisconsin–Madison, Madison, Wisconsin, U.S.A.). HIRS monthly cloud retrievals between 1979 and 2001. Personal Communication, November 2004.
17. Adler, R.F.; Huffman, G.J.; Chang, A.; Ferraro, R.; Xie, P.-P.; Janowiak, J.; Rudolf, B.; Schneider, U.; Curtis, S.; Bolvin, D.; et al. The Version-2 Global Precipitation Climatology Project (GPCP) monthly precipitation analysis (1979–present). *J. Hydrometeor.* **2003**, *4*, 1147–1167. [[CrossRef](#)]
18. Huffman, G.J.; Adler, R.F.; Bolvin, D.T.; Gu, G. Improving the global precipitation record: GPCP version 2.1. *Geophys. Res. Lett.* **2009**, *36*, L17808. [[CrossRef](#)]
19. Huffman, G.J.; Bolvin, D.T. *GPCP Version 2.2 SG Combined Precipitation Data Set Documentation*; Mesoscale Atmospheric Processes Laboratory and Science Systems and Applications, Inc.; NASA Goddard Space Flight Center: Greenbelt, MD, USA, 2013.
20. Adler, R.F.; Sapiiano, M.; Huffman, G.J.; Wang, J.; Gu, G.; Bolvin, D.; Chiu, L.; Schneider, U.; Becker, A.; Nelkin, E.; et al. The Global Precipitation Climatology Project (GPCP) Monthly Analysis (New Version 2.3) and a Review of 2017 Global Precipitation. *Atmosphere* **2018**, *9*, 138. [[CrossRef](#)]
21. Global Precipitation Climatology Project—Monthly, Version 2.3, NOAA Earth System Research Laboratory, Physical Sciences Laboratory. Available online: <https://www.esrl.noaa.gov/psd/data/gridded/data.gpcp.html> (accessed on 2 December 2019).
22. El Niño Southern Oscillation (ENSO), NOAA Earth System Research Laboratory, Physical Sciences Laboratory. Available online: <https://www.esrl.noaa.gov/psd/enso/enso.description.html> (accessed on 12 April 2017).
23. Oceanic Niño Index, NOAA Climate Prediction Center. Available online: http://www.cpc.ncep.noaa.gov/products/analysis_monitoring/ensostuff/ensoyears.shtml (accessed on 30 April 2016).
24. Southern Oscillation Index, Bureau of Meteorology. Available online: <http://www.bom.gov.au/climate/current/soi2.shtml> (accessed on 30 April 2016).
25. Ignatov, A.; Laszlo, I.; Harrod, E.D.; Kidwell, K.B.; Goodrum, G.P. Equator crossing times for NOAA, ERS and EOS sun-synchronous satellites. *Int. J. Remote Sens.* **2004**, *25*, 5255–5266. [[CrossRef](#)]
26. Udelhofen, P.M.; Gies, P.; Roy, C.; Randel, W.J. Surface UV radiation over Australia, 1979–1992: Effects of ozone and cloud cover changes on variations of UV radiation. *J. Geophys. Res.* **1999**, *104*, 19135–19159. [[CrossRef](#)]
27. Raut, B.; Jakob, C.; Reeder, M.J. Rainfall changes over Southwestern Australia and their relationship to the Southern Annular Mode and ENSO. *J. Clim.* **2014**, *27*, 5801–5814. [[CrossRef](#)]
28. Frey, R.A.; Menzel, W.P. Observed HIRS and MODIS High-Cloud Frequencies in the 2000s. *J. Appl. Meteor. Climatol.* **2019**, *58*, 2469–2478. [[CrossRef](#)]